Sixth International Symposium on Marine Propulsors
smp'19, Rome, Italy, May 2019

Cavitation Erosion Resistance Evaluation of Anti-erosion Coatings in Cavitation Tunnel

Hyoungsuk Lee[1], Sunghoon Kim[1], Heeyoung Choi[2], Sukjeong Lee[2], Bugeun Paik[3]

[1]Maritime Research Institute, Hyundai Heavy Industries (HHI), Seoul, Republic of Korea
[2]Advanced Technology Institutes, Hyundai Heavy Industries (HHI), Ulsan, Republic of Korea
[3]Advanced Ship Research Division, Korea Research Institute of Ships & Ocean Engineering (KRISO), Daejeon, Republic of Korea

ABSTRACT

To apply the anti-erosion coatings to the marine applications, such as rudder, composite marine propellers and etc., it is necessary to execute adequate test to evaluate the cavitation erosion resistance of the coatings.

Generally, the vibratory apparatus composed of a magnestostrictive oscillator is used according to the ASTM standard test method (G32 or G32M), which is a simple process to ensure rapid cavitation attack. Alternatively, the test in cavitation tunnel is conducted with specimens inserted in 2D hydro foil with obstacles attached to the leading edge for evaluating the erosion resistance of the coating. The test in the cavitation tunnel requires more complex test facilities and costs than the ASTM standard, but it is known to be the most adequate test method to reproduce cavitation conditions closer to the real situation of fluid-machinery.

With this background, the vibratory apparatus and the cavitation tunnel erosion test are compared for the anti-erosion coatings in this study.

Keywords

Anti-erosion, Coating, ASTM G32M, Cavitation tunnel.

1 INTRODUCTION

SUS plate cladding is commonly applied to prevent cavitation erosion of rudder. However, SUS is also responsible for galvanic corrosion due to the electric potential difference with the main material, mild steel. For this reason, several companies develop anti-erosive marine paints and commercialize them as alternatives to the SUS cladding.

Meanwhile, an application of Fiber-Reinforced-Plastic (FRP) to marine propellers instead of traditional metals (Nickel-Aluminum-Bronze (NAB), Manganese-Nickel-Aluminum Bronze (MAB)) is currently being investigated and manufactured because of the propulsion performance improvement, relative lightness and corrosion-resistance. Even though the cavitation inception speed of the FRP composite material propeller is much higher than that of metal propellers, the erosion resistance of FRP itself is much less than the metals. Therefore, it is essential for FRP propeller to be protected with coatings to endure cavitation erosion as well as penetration of seawater into FRP layer matrix.

For these reasons, it is necessary to evaluate the erosion resistance of the coatings before applying the coatings to the marine applications.

The cavitation erosion testing method commonly used in the laboratory scale is the vibratory cavitation apparatus because of its excellent convenience and reproducibility. In this test, the cavitation is generated by a vibratory oscillating horn. This test method is divided into the "direct" method (ASTM G32), which uses the collapse of the micro bubble cloud generated from the specimen face by vibrating the horn with the specimen, and the "alternative" method (ASTM G32M), which uses the collapse of the micro bubble cloud between the vibrating dummy button and the fixed specimen.

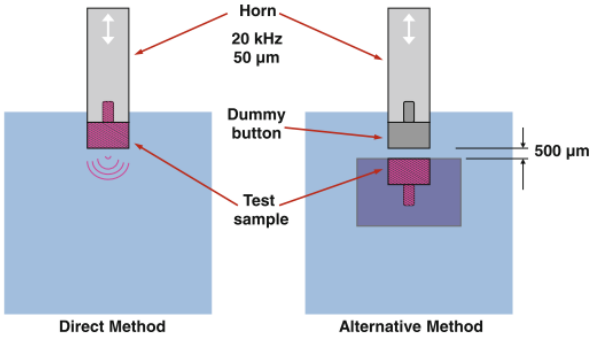

Figure 1 The test setups for the ultrasonic ASTM G32 direct method (left) and ASTM G32M alternative method (right) (Chahine et al., 2014a)

Even though the vibratory apparatus methodology presents a simple usage and it ensures rapid cavitation attack, it is limited to quantify the cavitation erosion that occurs in marine applications considering an unrealistic cavitation is generated because the actual hydrodynamic conditions are not simulated properly. As an alternative to these methods, the cavitation tunnel test with vortex

cavitation generating obstacles (VCGO) attached 2D hydro foil is available. In this test method, the special facilities (high speed cavitation tunnel) are required and time costs for the test are relatively high, the process from cavitation inception to collapse is reproduced in the flow, and the pattern of erosion caused by this test is the same as the actual phenomenon.

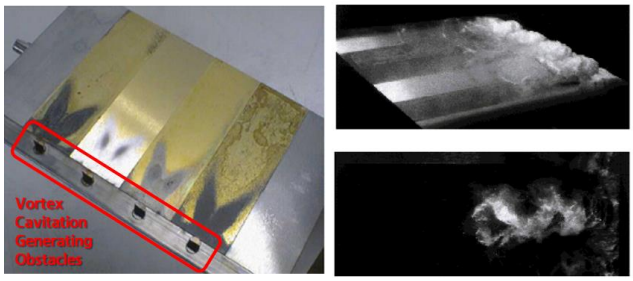

Figure 2 Eroded specimens after 75 hour cavitation test (left) and flow visualization of the cavitation pattern (right) at U_{inf} = 35 m/s, σ = 1 and α = 3° (Escaler et al., 2003)

In this study, the anti-erosion tests are performed on two kinds of urethane-based anti-erosion coating materials and comparative materials. Commonly used ASTM G32M method and the erosion test in cavitation tunnel are carried out and differences in each test are compared. Due to the limitation of long time operable flow velocity of the cavitation tunnels, the testing rig including specimens, VCGO and foil is newly designed in order to maximize the intensity of cavitation.

2 ASTM VIBRATORY APARATUS TEST

To verify the cavitation erosion resistance of the anti-erosion coatings, the well-known ASTM G32M vibratory apparatus method is applied.

2.1 Test Set-up

The settings and procedures of the test are in accordance with the ASTM G32 alternative method. The following figure shows the configuration of the system used in this study.

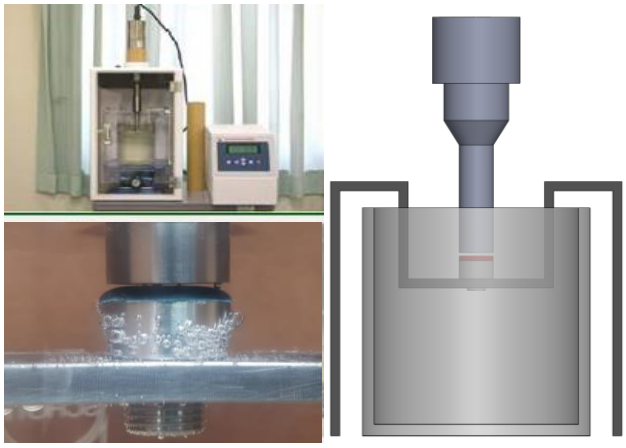

Figure 3 ASTM G32M vibratory apparatus cavitation erosion test set-up

2.2 Materials

Tests are carried out to evaluate the erosion resistance performance of two anti-erosion coatings: a polyurethane based paint (coating A) and an elastomer coating whose major components were not disclosed (coating B). And an anti-erosion performance evaluation of coating C is carried out at the same time, which is widely applied to marine applications including ship hull, as a comparison material for the coating materials. The coating C is not designed to resist cavitation erosion. Base material composition and characteristics of the coating A, B and C are shown in Table 1.

Table 1 Material characteristics of coatings applied to ASTM vibratory test

	Base composition	Application method	Density (g/cm^3)
Coating A	Polyurethane	spray	1.017
Coating B	Elastomer	brush	1.035
Coating C (ref.)	Vinyl Ester + Glass Flake	spray	1.240

2.3 Results and Discussion

The cumulative mass losses over testing time for the three kinds of specimens are shown in Figure 4.

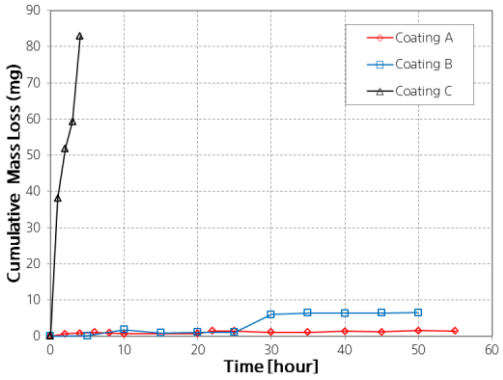

Figure 4 Cumulative mass losses of each coating

Since there are differences in density, it is not appropriate to evaluate the anti-erosion performance of each material by comparing the accumulative mass losses. Therefore, it is more suitable to compare the volumes of the eroded material, and the cumulative volume losses (Figure 5) are derived using the density of each material (Table 1).

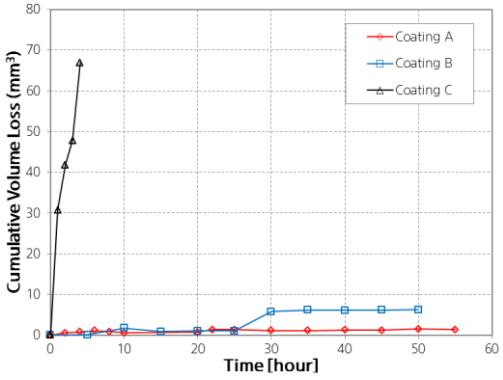

Figure 5 Cumulative volume losses of each coating

The cavitation erosion resistance of the anti-erosion coatings (A and B) is relatively superior to that of the reference material (coating C), which had a volume loss of 66.85 mm ^{3} within 4 hours after the start of the test. At the beginning of the test, the volume loss of coating A and B proceeded to a similar extent, and the volume loss of coating B increased suddenly from 1.06 mm^3 to 5.80 mm^3 between 25 hours and 30 hours. The volume loss in this period is about 0.95 mm^3 per hour, and it is much larger than the highest loss per hour, 0.20 mm^3 at initial test stage. This is presumably due to the small damage drop of the coating surface due to the cavitation impact rather than the volume change due to erosion pitting. Coating B shows a volume loss rate similar to coating A again after a large amount of coating volume loss. From these results, cavitation erosion pitting resistance of coating A and B is a similar level, but the amount of the coating losses is different, so a more rigorous test is required.

3 EROSION TEST AT CAVITATION TUNNEL

Although the ASTM standard testing method is widely used due to the repeatability and availability of the test, there is a physical difference from the actual mechanism that cavitation occurs, develops and collapses.

In order to reproduce the conditions more similar to actual phenomena of cavitation erosion, the high speed cavitation tunnel test performed by Escaler et al. (2003) is redesigned to meet the test facility conditions of this study and the erosion resistances for the anti-erosion coatings are performed.

3.1 Testing Facility, Rig and Methodology

This test was conducted in a high-speed cavitation tunnel of Korea Research Institute of Ships & Ocean Engineering (KRISO). The specifications of the test section of the cavitation tunnel are as follows.

length×width×depth: 3.0 m × 0.3 m × 0.3 m

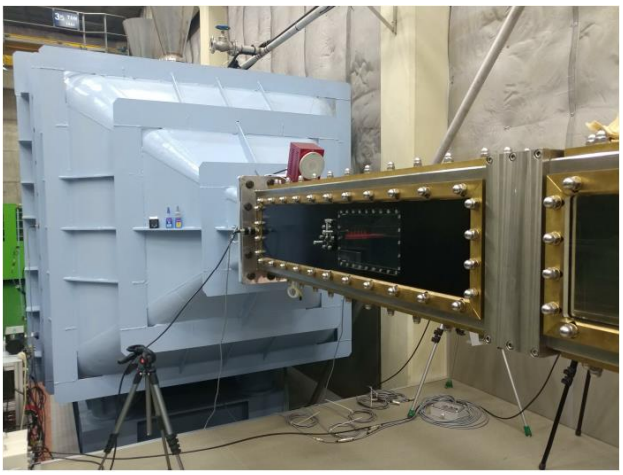

Figure 6 Test section of cavitation tunnel of Korea Research Institute of Ships & Ocean Engineering (KRISO)

The maximum velocity of the KRISO cavitation tunnel is 20.4 m/s, and the operation pressure is from 0.2 atm (Kgf/cm^2) to 2.0 atm. Although the maximum velocity of the high-speed cavitation tunnel is 20.4 m/s, it is limited to the maximum operating speed of 13.0 m/s during the test considering the durability of the tunnel because the test needs to be conducted for a long time until erosion on the specimens occurs and develops. A photograph of the test section of the KRISO high-speed cavitation is shown in Figure 6.

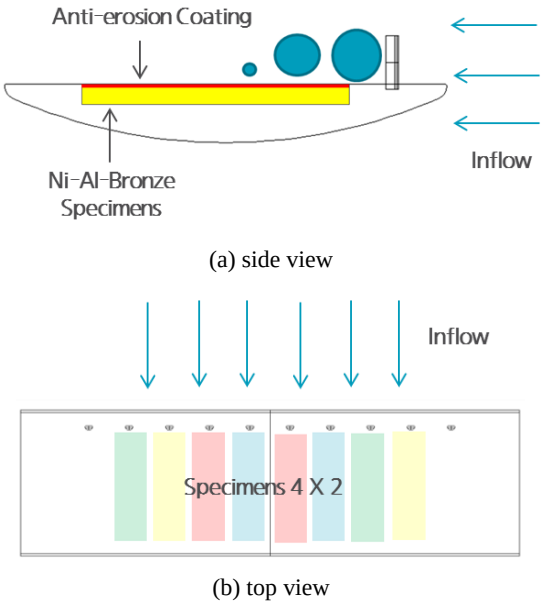

Figure 7 Schematic diagrams of foil with VCGO and specimens

3.2 Materials

The materials used in the cavitation tunnel test are coatings A and B which had been already applied to the vibratory apparatus test. The comparative reference materials are selected as NAB which is used as the main material of commercial propeller, and coating D which is widely applied as an anti-erosion paint for marine applications such as rudder.

Table 2 Material characteristics of anti-erosion coatings applied to cavitation test in KRISO cavitation tunnel

	Base composition	Application method	Density (g/cm^3)
Coating A	Polyurethane	spray	1.017
Coating B	Elastomer	brush	1.035
NAB (ref.)	Ni-Al-Br metal	-	7.530
Coating D (ref.)	Urethane modified epoxy	brush	1.130

3.3 Design of Testing Rig and Condition

The area of the test section of the KRISO tunnel is four times larger than that of the EPFL tunnel, which means that the number of specimens that can be tested at one time is twice as large. However, in order to ensure enough cavitation intensity to cause erosion in spite of the relatively low operating flow speed, it is necessary to dispose of the conditions including the test rig design. Therefore, the CFD analysis using commercial software, StarCCM+, is performed for various cases to determine

the optimal test equipment configuration and conditions for the erosion test in the KRISO tunnel.

3.3.1 Reference Case Study

Based on the Escaler's test (2003), the geometry and conditions of the equipment are determined to simulate as the actual cavitation characteristics as much as possible. The shape of the plane-convex hydrofoil equipped with obstacles used in the reference case is shown in the following figure. The test was performed for pairs of two material specimens, cermet and stainless steel.

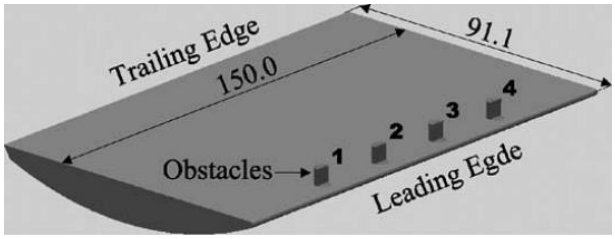

Figure 8 Outline of the 2D plane-convex hydrofoil with the semi-cylindrical surface-mounted obstacles in front of the specimens (Escaler et al., 2003)

In order to verify the applicability of CFD analysis based design, the detached-eddy simulation (DES) is used for simulating highly unsteady turbulent flow. For a calculation of cavity flow, a multi-phase mixture model assuming that a working medium is a single fluid with a homogeneous mixture of two phases (liquid and vapor) is used. Schnerr and Sauer model (2001) is used for the cavitation model for the simulation. Detailed information for numerical simulation is shown in Table 3.

Table 3 Numerical simulation setting

Turbulence model	IDDES (DES)
Cavitation model	Schnerr-Sauer (S-S)
Temporal discretization	2nd order implicit
Time step	10 μs
No. of grid	abt. 10 million

In order to predict the strength of cavitation erosion, several erosion indices proposed by Naomi (2008). The indices are shown in the following expressions (1) and (2). Each expression assumes that erosion may occur on the surface that cavity void fraction is high and the level of the pressure change is high.

$$\text{Index A} = \alpha \cdot \max\left[p - p_v, 0\right] \tag{1}$$

$$\text{Index B} = \max\left[-\frac{\partial p}{\partial t}, 0\right] \tag{2}$$

The numerical simulation is performed under the test conditions of inflow velocity (U_{inf}) 35 m/s, cavitation number (σ) 1.0 and flow angle of attack (α) 3°, and CFD analysis result are shown in Figure 9. The accumulating plots of erosion indices on foil (specimens) surface from 0 sec. to 0.02 sec. are shown in Figure 10. As shown in Figure 9, the cavitation flow pattern of the analysis is simulated similar to the pattern of the experiment, so that it is possible to derive the optimal experimental conditions based on the maximum pressure and erosion index obtained by the CFD methodology.

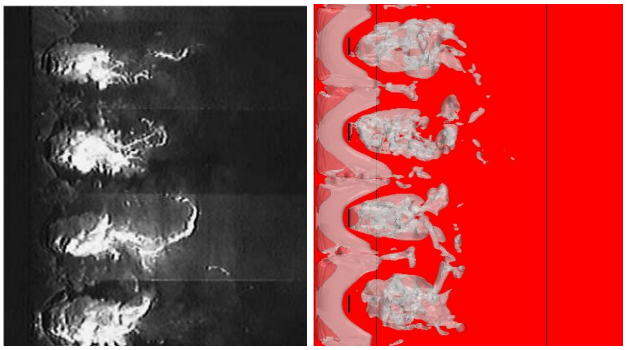

Figure 9 View of a cavitation flow of the cavitation test (left) and CFD simulation (right)

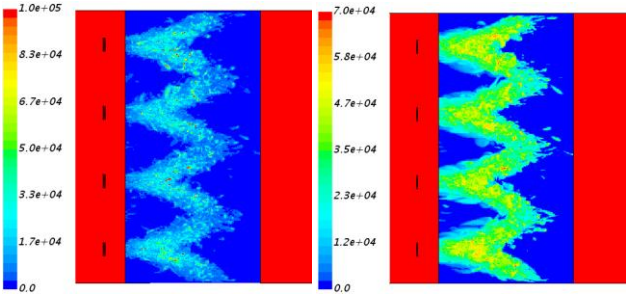

Figure 10 The accumulating plots of erosion index A (left) and erosion index B (right) for reference case

3.3.2 Initial Design of Test Rig

The test rig foil design has been determined through analysis of the various sizes, shapes and arrangements of obstacles and flow angle of attacks, and it is shown in Figure 11. A total of 10 semi-cylindrical obstacles are set up near leading edge to accommodate eight test specimens.

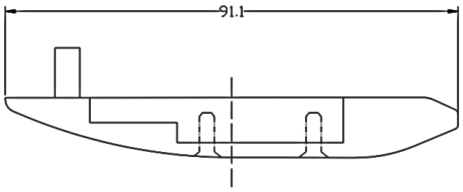

(a) section view

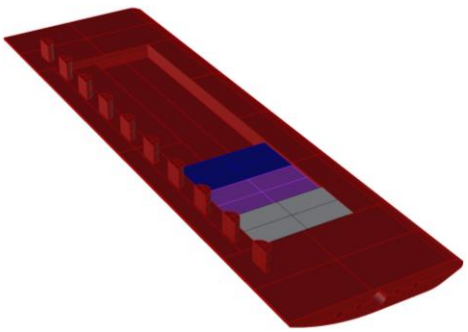

(b) perspective view

Figure 11 Testing rig (hydrofoil, VCGOs and specimens) design for cavitation test at KRISO tunnel

The condition with cavitation number 0.8, vapor pressure of fresh water (at 15^{o} C) 1,750 Pa and flow angle of attack 3^{o} is expected as the most severe one at the flow velocity of 13.0 m/s. The accumulating plots of erosion indices of the condition are shown in Figure 12, and comparisons of maximum pressure and erosion index A between Escaler's reference case and designed case are shown in Figure 13. The erosion index B also showed a similar tendency to the erosion index A. In the absence of quantification of erosion for each indicator, quantitative comparisons are insignificant. However, considering overall trends such as differences in maximum pressure over time history, additional rig design and test setting improvements are required.

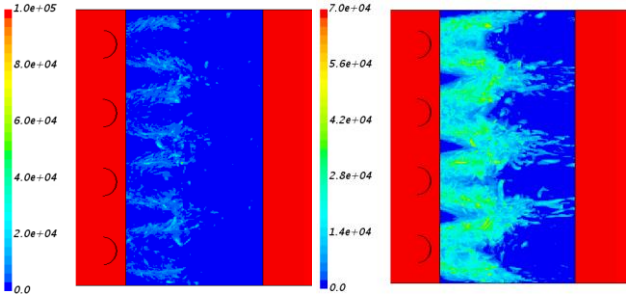

Figure 12 The accumulating plots of erosion index A (left) and erosion index B (right) for initial design

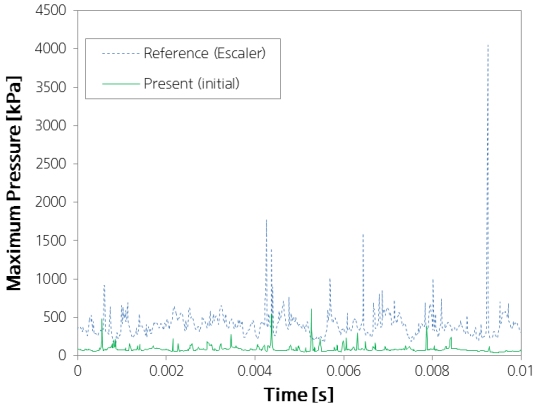

(a) maximum pressure

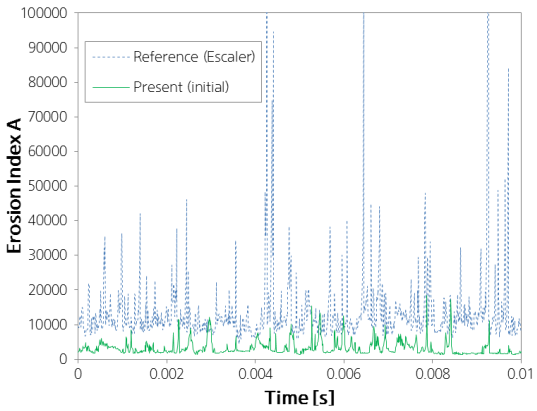

(b) erosion index A

Figure 13 Comparisons of simulated cavitation characteristic between reference and initial design

3.3.3 Modified Design of Test Rig

To facilitate the increase of cavitation erosiveness, an additional hydrofoil is placed above the leading edge of the existing foil rig and the flow angle attack is increased by 5^{o}.

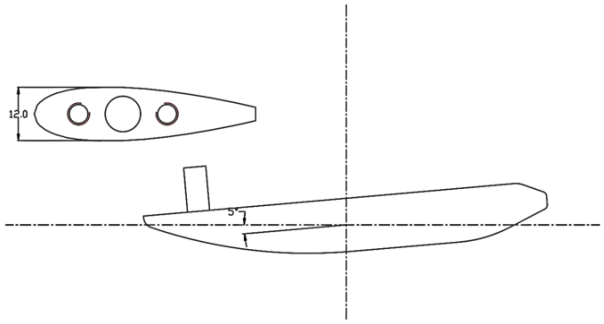

Figure 14 Modified testing rig design for cavitation test at KRISO tunnel

Figures 15 through 17 show the results of the analysis for the modified conditions. Although the level of index A still does not reach the level from the reference case, the modified design case shows improved tendency rather than initial design, so we conducted erosion resistance test on the modified design.

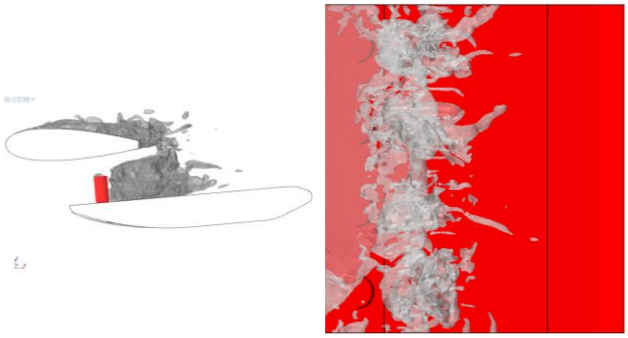

Figure 15 CFD stimulation of modified rig setting (left: side view, right: top view)

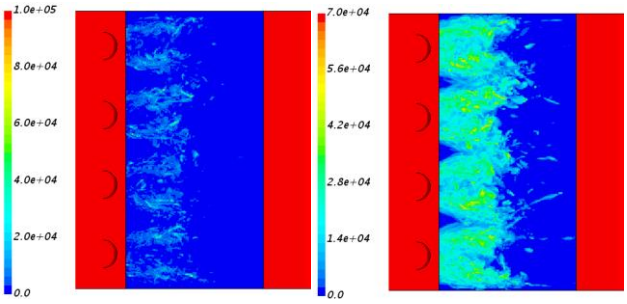

Figure 16 The accumulating plots of erosion index A (left) and erosion index B (right) for modified design

3.4 Test Setting of Cavitation Tunnel Test

Since the condition of the test is very severe for the operation of the cavitation tunnel, the water temperature inside the tunnel is gradually increased due to the friction between the tunnel and the water, and overheating of the impeller bearing. Therefore, the continuous operation time of the tunnel is limited within 3 to 7 hours. After continuous operation, the specimens are sufficiently dried to remove moisture and the mass histories of each

specimen are measured using a high precision micro mass meter. (ABJ220 supplied by Kern in Germany) Based on the measurement, we evaluated anti-erosion performance for each material.

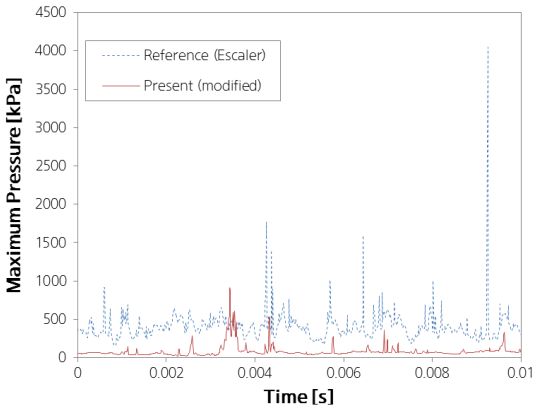

(a) maximum pressure

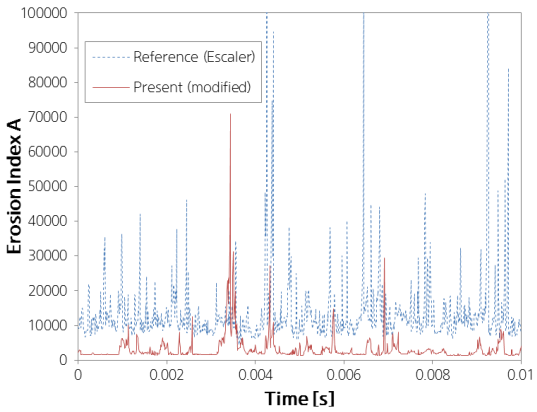

(b) erosion index A

Figure 17 Comparisons of simulated cavitation characteristic between reference and modified designed

As shown in the Figure 18, pairs of specimens of coating A, B and comparative materials (NAB and coating D) are randomly installed and the specimens array are moved side by one side in sequence after every 3-7 hours during the erosion test to eliminate errors that may occur due to the limitation of tunnel and test rig.

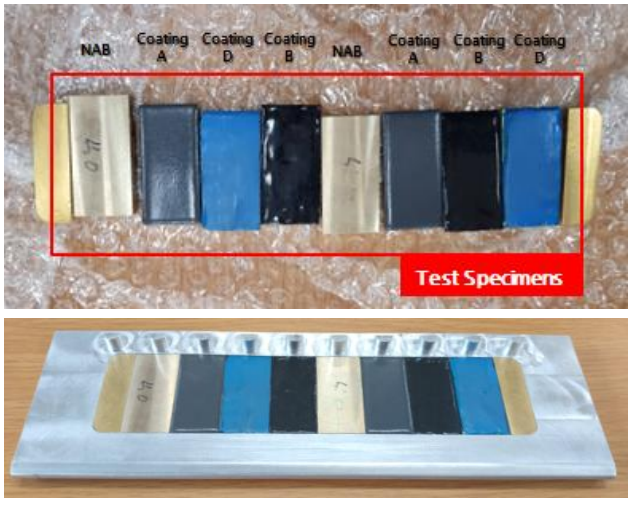

Figure 18 Reference array sequences of specimens

All specimens are fabricated with NAB material, and the coated specimens are manufactured with consideration of coating thickness to flatten the rig surface. Figure 19 shows the test rig installed in the tunnel.

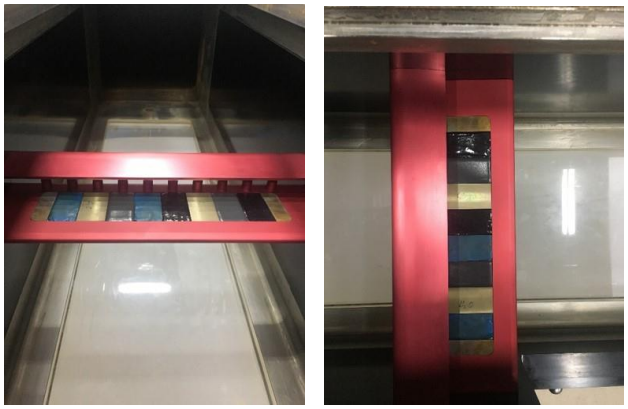

Figure 19 Test setting of cavitation tunnel test

3.5 Results and Discussion

Figure 20 shows observed cavitation patterns at the test condition, cavitation number of 0.8 and test flow velocity of 13 m/s. As predicted by the CFD analysis at design stage, sheet cavitation occurred due to excessive pressure drop at the surface of the additional upper hydrofoil, and it was confirmed that strong cavitation collapsed on the coated specimen due to the wedge obstacles installed at leading edge of the below foil rig. The test is carried out for 74 hours.

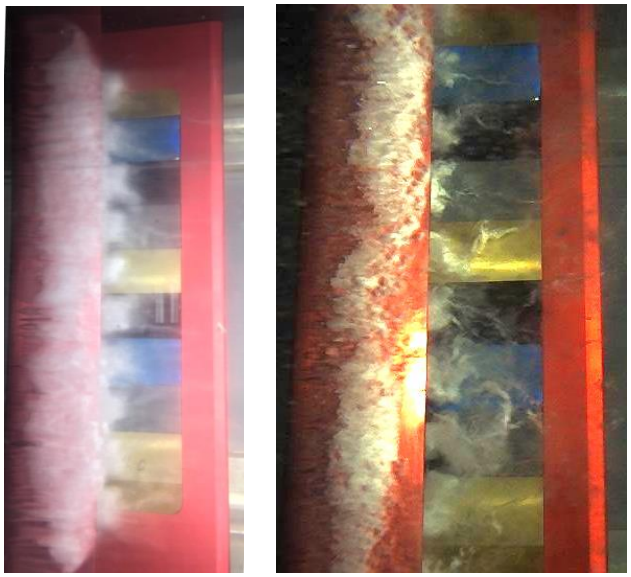

Figure 20 Snapshot of cavitation flow of still camera (left) and high-speed camera with 5,000 fps (right)

3.5.1 Mass Loss and Volume Loss

The cumulative mass losses over testing time for the four kinds of specimens are presented in Figure 21. The indicated amounts of mass loss are the average value of each pair. In spite of time increment, decrease or sudden increase of mass loss can be observed. One of the reasons is assumed that the specimen is not sufficiently dried at the measurement.

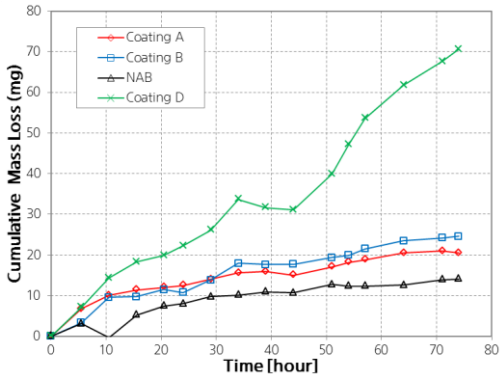

Figure 21 Cumulative mass loss of each specimen

However, some of these abnormal data do not seriously impair the tendency of the mass loss over testing time of the whole data

To compare the volumes of the eroded material, the cumulative volume losses (Figure 22) are derived using the density of each material (Table 2).

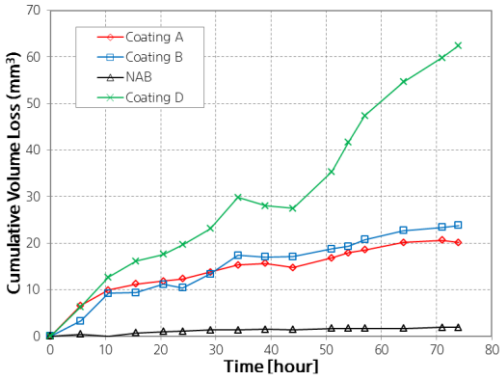

Figure 22 Cumulative volume loss of each specimen

3.5.2 A Review of the Results

At the end of the 74 hours of testing, the measured total mass losses for each material are 20.5 mg (coating A), 24.6 mg (coating B), 14.1 mg (NAB) and 70.6 mg (coating D). The volume losses are converted into 20.1 mm^3 (coating A), 23.8 mm^3 (coating B), 1.9 mm^3 (NAB) and 62.4 mm^3 (coating D), respectively. Coating A has about 20% better erosion resistance than B in volume loss, but considering the overall data trend, coating A and B are similar in erosion amount, and NAB is 1/10 and coating D is 3 times of those.

Similar to the ASTM vibratory apparatus test results, a sudden loss of the coating occurred at the initial stage and between 25 hours and 35 hours of cumulative testing time in the case of coating B. However, global mass or volume decrease patterns and rates show similar to coating A and B.

This testing method is more difficult and expensive than the ASTM G32M method, even though the tendency for cavitation erosion resistance for coating A and B between the two tests is similar. Nevertheless, the cavitation tunnel test is considered to be more reliable because the physical mechanism of erosion due to the occurrence and collapse of cavitation is the same as the actual mechanism. In addition, it can be concluded that more rigorous results can be derived, as the erosion resistance test for each material can be carried out simultaneously.

4 CONCLUSIONS

To evaluate the erosion resistance of the two kinds of anti-erosion coating materials (coating A and B), the widely used alternative ASTM G32M method and the cavitation tunnel test, which reflect the actual cavitation mechanism of marine applications, are performed. In each test, glass platelets reinforced vinyl ester resin coating (coating C) and NAB / urethane modified epoxy based coating (coating D) are used as the comparative materials to evaluate the performance of the target materials.

ASTM G32M vibratory apparatus tests for coating A, B and C are carried out in accordance with the standard procedure. Cavitation tunnel test are also carried out with specimens with VCGOs attached hydrofoil type rig.

In order to maximize and accelerate cavitation erosion for the cavitation tunnel test, even under relatively slow tunnel flow conditions, a test set up consisting of main hydrofoil equipped with specimens and VCGOs and additional hydrofoil are designed by CFD analysis. During the test, eight different specimens are attacked by collapsing cavitation simultaneously, and the position of the specimens had been changed sequentially during the test in order to minimize the positional effects due to asymmetry in the test. As the test progressed, the mass and volume loss change of the specimens are measured, and the erosion resistance performances are evaluated.

As results of ASTM G32M test and cavitation tunnel test, though they are not as better as NAB, the target materials are similar to each other and are found to be superior in cavitation erosion resistance to reference materials, coating C and D.

Both test methodologies showed similar results, therefore the usefulness of the cavitation tunnel test for evaluating the erosion resistance of the anti-erosion coating can be confirmed.

REFERENCES

Basumatary, J. (2017). Cavitation erosion-corrosion in marine propeller materials. Doctoral Thesis, University of Southampton, UK.

Chahine, G.L., Franc, J.-P., & Karimi, A. (2014a). 'Laboratory Testing Methods of Cavitation Erosion', Chapter 2, in Kim, K-H, Chahine, G.L., Franc, J-P., Karimi, A. (eds): Advanced Experimental and Numerical Techniques for Cavitation Erosion Prediction, Springer, Berlin.

Chahine, G.L., Franc, J.-P., & Karimi, A. (2014b). 'Cavitation Impulsive Pressures', Chapter 4, in Kim, K-H, Chahine, G.L., Franc, J-P., Karimi, A. (eds): Advanced Experimental and Numerical Techniques for Cavitation Erosion Prediction, Springer, Berlin.

Dular, M., Bachert, B., Stoffel, B. & Širok, B. (2004). 'Relationship between Cavitation Structures and Cavitation Damage', Wear **257**.

Dular, M. & Petkovšek, M. (2015). 'On the Mechanisms of Cavitation Erosion - Coupling High Speed Videos to Damage Patterns', Experimental Thermal and Fluid Science **68**.

Escaler, X., Avellan, F. & Egusquiza, E. (2001). 'Cavitation Erosion Prediction from Inferred Forces using Material Resistance Data', Proceedings of Forth International Symposium on Cavitation (CAV2001), California, USA.

Escaler, X., Farhat, M., Avellan, F. & Egusquiza, E. (2003). 'Cavitation Erosion Tests on a 2D Hydrofoil using Surface-mounted Obstacles', Wear **254**.

Nohmi, M., Iga, Y. and Ikohagi, T. (2008) 'Numerical Prediction Method of Cavitation Erosion', Conference Proceeding of Turbomachinery Societh of Japan **59**, pp. 49-54.

Paik, B-G, Kim, K-S, Kim, K-Y, Ahn, J-W, Kim, T-K, Kim, K-R, Jang, Y-H & Lee, S-U (2011) 'Test Method of Cavitation Erosion for Marine Coatings with Low Hardness', Ocean Engineering **38.**

Schnerr, G. H. and Sauer J. (2001). 'Physical and Numerical Modeling of Unsteady Cavitation Dynamics', Proceedings of Fourth International Conference on Multiphase Flow, New Orleans, USA.

Tomov, P. (2016). Etude expérimentale et numérique de la cavitation et la cavitation aérée. Vers une application à l'alimentation en carburant d'un moteur d'avion. Doctoral Thesis, ParisTech, France.